Paleoceanography and Paleoclimatology

RESEARCH ARTICLE
10.1029/2020PA004172

Deglacial Ventilation Changes in the Deep Southwest Pacific

Yuhao Dai[1,3], Jimin Yu[1], and Patrick A. Rafter[2]

[1]Research School of Earth Sciences, Australian National University, Canberra, ACT, Australia, [2]Department of Earth System Science, University of California, Irvine, CA, USA, [3]Now at Department of Geology, Lund University, Lund, Sweden

Key Points:

- We present a new LCDW-depth radiocarbon record in the SW Pacific, with the deglacial age model constrained by tuning SST to Antarctic δD
- Two-phase ventilation increases at our core coincided with millennial-time scale atmospheric CO_2 rises during HS1 and the YD
- We show that the deep SW Pacific became less well ventilated and more stratified during the ACR, possibly due to the sea-ice readvancement

Supporting Information:

- Supporting Information S1

Correspondence to:

Y. Dai and J. Yu,
yuhao.dai@geol.lu.se;
jimin.yu@anu.edu.au

Citation:

Dai, Y., Yu, J., & Rafter, P. A. (2021). Deglacial ventilation changes in the deep Southwest Pacific. *Paleoceanography and Paleoclimatology*, *36*, e2020PA004172. https://doi.org/10.1029/2020PA004172

Received 24 NOV 2020
Accepted 11 JAN 2021

Abstract Processes underlying changes in the oceanic carbon storage during the Last Glacial Maximum and the subsequent deglaciation are not fully understood. Here, we present a new high-resolution radiocarbon reconstruction (expressed as $\delta^{14}R$) at the depth of the modern Lower Circumpolar Deep Water from the Pacific Sector of the Southern Ocean. Our record shows $\delta^{14}R$ increases during Heinrich Stadial 1 and the Younger Dryas that agree with the deep-to-shallow transfer of old carbon in the Southern Ocean during these two periods. Our record also shows, for the first time, a clear ~80‰ decline in $\delta^{14}R$ during the Antarctic Cold Reversal (ACR), indicating the development of poorly ventilated conditions in the deep Southwest Pacific. These conditions are consistent with the increased Southern Ocean sea-ice and associated stratification between Upper and Lower Circumpolar Deep Waters. This enhanced stratification in the deep South Pacific possibly facilitated greater carbon storage in the ocean interior during the ACR, effectively limiting oceanic CO_2 release and contributing to the atmospheric CO_2 plateau as observed in ice cores at that time.

1. Introduction

Atmospheric CO_2 increased by about 90 ppm from the Last Glacial Maximum (LGM; 22 to 18 kyr) to the late Holocene (Marcott et al., 2014; Monnin et al., 2001; Petit et al., 1999). The ocean is thought to be a major source for the deglacial atmospheric CO_2 rise due to its large carbon storage (Sigman & Boyle, 2000; Sigman et al., 2010, and references therein). The Southern Ocean possibly plays an important role in affecting atmospheric CO_2, because it is a region where CO_2-rich deep waters outcrop and exchange carbon with the atmosphere, a process termed as ventilation (Sarmiento & Toggweiler, 1984). Existing data indeed show coupling of Southern Ocean upwelling and ventilation with atmospheric CO_2 changes during the last deglaciation (Anderson et al., 2009; Burke & Robinson, 2011; Skinner et al., 2010; Yu et al., 2010). For example, atmospheric CO_2 increased during Heinrich Stadial 1 (HS1; ~18.0–14.6 kyr) and the Younger Dryas (YD; ~12.8–11.7 kyr), synchronous with Southern Hemisphere warming (Monnin et al., 2001). During these time periods, upwelling in the Southern Ocean strengthened (Anderson et al., 2009), accompanied by sea-ice retreat (Lamping et al., 2020; EPICA Community Members, 2013). By contrast, there was a pause in atmospheric CO_2 rise during the Antarctic Cold Reversal (ACR; ~14.6–12.8 kyr) (Marcott et al., 2014), a period with widespread cooling at mid-high latitudes in the Southern Hemisphere (Pedro et al., 2015), reduced Southern Ocean upwelling (Anderson et al., 2009), and sea-ice expansion (Lamping et al., 2020; EPICA Community Members, 2013).

Pioneered by Broecker (Broecker et al., 1988), measurements of radiocarbon in marine carbonates provide critical information about deglacial ventilation changes in the Southern Ocean (Barker et al., 2010; Burke & Robinson, 2011; Ronge et al., 2020; Rose et al., 2010; Sikes et al., 2000, 2016; Skinner et al., 2010, 2015). Published data indicate enhanced ventilation and probable release of old carbon at various water depths from the Southern Ocean (Burke & Robinson, 2011; Hines et al., 2015; Skinner et al., 2010). Moreover, seawater radiocarbon signals at different depths converged during the early deglaciation, implying a breakdown of the Southern Ocean stratification (Burke & Robinson, 2011; Hines et al., 2015; Ronge et al., 2016; Skinner et al., 2010) and the release of carbon from the Southern Ocean to the atmosphere (Allen et al., 2015; Rae et al., 2018). However, the deep Southern Ocean ventilation changes are not well constrained during the late deglaciation. The exact temporal evolution history of deep-water radiocarbon in the Pacific Sector of the Southern Ocean remains largely unknown, due to the lack of high-resolution records (e.g., Sikes

et al., 2016; Skinner et al., 2015). A recent low-resolution record from the Indian Sector of the Southern Ocean shows old deep-water radiocarbon during the ACR and young deep-water radiocarbon during the YD (Ronge et al., 2020). These results differ from the deep South Atlantic reconstructions, which show small radiocarbon variability since the ACR (Skinner et al., 2010). Given the large volume and the substantial carbon stock of the Pacific Ocean, filling the gap of deep-water radiocarbon data in the Pacific Sector of the Southern Ocean is critical to improve our understanding about past carbon cycle changes.

Deep-water radiocarbon signatures can be reconstructed using various archives including foraminifera shells (see Broecker et al., 1988) and deep-sea corals (see Adkins & Boyle, 1997). Each archive has its pros and cons, and may record different aspects of seawater radiocarbon changes. While deep-sea corals allow absolute U-Th dating (Burke & Robinson, 2011; Chen et al., 2015; Hines et al., 2015), their temporal and spatial distribution is limited (Hines et al., 2015), and, as a result, continuous records are currently sparse. Conversely, foraminiferal radiocarbon records may suffer from age model uncertainties, although they can provide continuous down-core records. For example, potential surface reservoir age fluctuation is a large source of uncertainty for deep water radiocarbon calculations, if the sediment core's age model relies on radiocarbon dating of planktic foraminifera. Sediment core age models may be substantially improved using wood remains and tephra layers, but such records are geographically limited (Rafter et al., 2018; Siani et al., 2013; Sikes et al., 2000; Skinner et al., 2015; Zhao & Keigwin, 2018). Regardless of materials used, recent studies show that deep-water radiocarbon reconstructions could be further complicated by possible release of ^{14}C-depleted carbon from local geological settings (Lizarralde et al., 2010; Rafter et al., 2019; Ronge et al., 2016; Stott et al., 2019).

Here, we present a high-resolution record for deep-water radiocarbon signatures for the Southwest Pacific Ocean. Our new radiocarbon record lends support to the deglacial release of old carbon from the deep Southern Ocean during HS1 and the YD. More importantly, our data suggest that the ventilation of the deep Southwest Pacific was reduced during the ACR. Combined with published results, we argue that the deep Southern Ocean became more stratified during the ACR compared to the early last deglaciation. Our record demonstrates that deglacial atmospheric CO_2 change was closely linked to the deep Southern Ocean ventilation.

2. Material and Analytical Methods

2.1. Modern Hydrography

The sediment core MD97-2106 (45.15°S, 146.28°E, 3,310 m) is located on the South Tasman Rise (Figure 1), which is not influenced by any known seafloor volcanism and subduction that are potentially linked to release of ^{14}C-depleted carbon. The core is currently positioned near the Subtropical Front (STF) (Sokolov & Rintoul, 2002; Talley, 2011). Because the STF migrated northwards during the LGM in this region (e.g., Bostock et al., 2015; Sikes et al., 2009), surface hydrology at the core location was dominated by Subantarctic surface waters during the last deglaciation. This allows us to establish an age model by tuning sea surface temperature (SST) at the core location to Antarctic air temperature (e.g., Pahnke et al., 2003; Ronge et al., 2016; Rose et al., 2010; Waelbroeck et al., 2019). Regarding deep water conditions, core MD97-2106 is currently bathed in Circumpolar Deep Water (CDW) (Figure 1b), a mixture of deep waters from all three major ocean basins and Antarctic Bottom Water (AABW) (Talley, 2011, 2013). The lower CDW (LCDW) upwells to the South of the Antarctic Circumpolar Current. A branch of the upwelled waters is transported southwards, some of which eventually sinks and contributes to AABW (Rintoul, 2018; Talley, 2011, 2013). Recent modeling studies suggest that most AABW recirculates within the Southern Ocean, and only a small portion is transported northwards into the Indo-Pacific Ocean (Farneti et al., 2015; Lee et al., 2019). Compared to LCDW, the upper CDW (UCDW) upwells further north in the Antarctic Zone. After upwelling, UCDW subsequently subducts and is transported mostly northwards, contributing to intermediate and mode water formations (Talley, 2011, 2013). Because core MD97-2106 is bathed in LCDW, this site can be used to investigate the ventilation of the deep Southern Ocean.

2.2. Planktic Mg/Ca

SST at MD97-2106 is reconstructed using Mg/Ca in the planktic foraminifera *Globigerina bulloides*. From each sample, about 30–40 foraminifera shells from the 300–355 μm size fraction were picked and cleaned

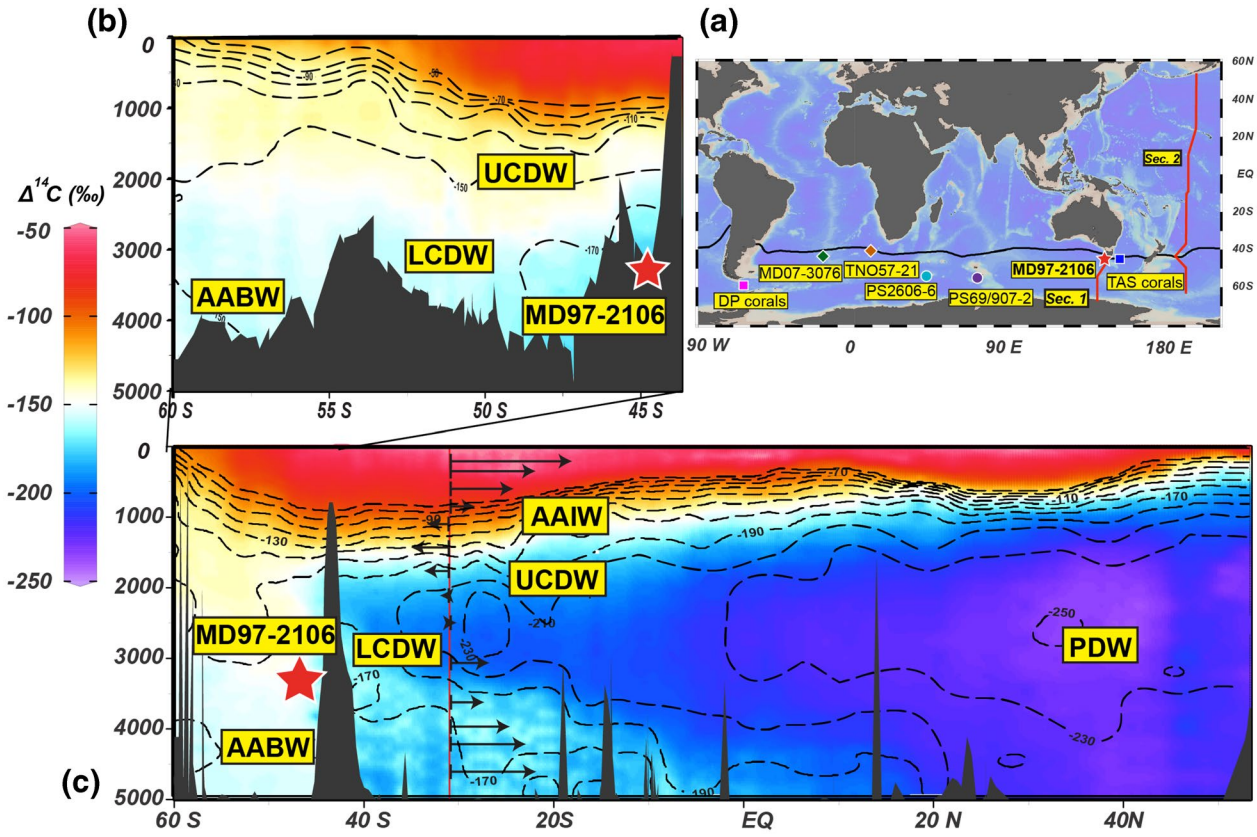

Figure 1. (a) Location of core MD97-2106, and other records discussed in the paper. The black curve represents the annual mean position of the modern STF. (b) Natural seawater $\Delta^{14}C$ transect along sections 1 shown in (a). (c) The same as (b) but for section 2 (Key et al., 2004). Black arrows in (c) indicate modern water transport across 32°S in the Pacific (Ganachaud, 2003). STF, Subtropical Front. AABW, Antarctic Bottom Water; LCDW, Lower Circumpolar Deep Water; UCDW, Upper Circumpolar Deep Water; AAIW, Antarctic Intermediate Water; PDW, Pacific Deep Water.

following the "Mg-cleaning" procedure without the "reductive-cleaning" step (Barker et al., 2003; Boyle & Keigwin, 1985). The "Mg-cleaning" procedure is chosen to prevent potential partial dissolution during the reductive-cleaning step (Yu et al., 2007). Mg/Ca ratios, along with other element to calcium ratios, were measured on an iCAP RQ inductively coupled plasma mass spectrometer (ICP-MS) at the Australian National University (ANU), following an established method (Yu et al., 2005). Analytical precision for Mg/Ca is better than 1% (1 standard deviation, 1σ). Repeated measurements of carbonate reference materials, BAM RS3 and CMSI 1767, yield ratios (0.788 ± 0.004 mmol/mol, n = 10, 1σ and 5.56 ± 0.05 mmol/mol, n = 8, 1σ, respectively) comparable to the accepted values (Greaves et al., 2008). Al/Ca and Mn/Ca, which are measured to monitor effectiveness of the cleaning procedure, are below 40 and 30 μmol/mol, respectively, and neither of them correlates with Mg/Ca (Table S2). Mg/Ca-based SST is calculated using the calibration of Elderfield and Ganssen (2000).

2.3. Age Model

Our age model for MD97-2106 is based on combined use of planktic radiocarbon (Holocene and the LGM) and *G. bulloides* Mg/Ca-SST (the last deglaciation). The ages of the Holocene are constrained based on planktic foraminifera radiocarbon dates using a surface reservoir age of 500 ± 100 years (Moy et al., 2006). The ages of the LGM are calculated using planktic radiocarbon dates (Moy et al., 2006, this study) with a surface reservoir age of 1,155 ± 500 years following Skinner et al. (2017). A larger uncertainty for the LGM surface reservoir age is employed to account for less constraint on glacial surface reservoir age in the Southwest Pacific. These radiocarbon ages are calibrated using the IntCal20 curve (Reimer et al., 2020). To circumvent age uncertainties associated with potentially large surface reservoir age variability in the

South Pacific as previously reported (Sikes & Guilderson, 2016; Skinner et al., 2015), we avoid using age controls based on planktic radiocarbon during the last deglaciation. Instead, we construct the deglacial age model for MD97-2106 by aligning *G. bulloides* Mg/Ca-SST with the EPICA Dome C (EDC) δD record (Jouzel et al., 2007) on the WD2014 age model (Buizert et al., 2018; EPICA Community Members, 2006) (Figures 2c and 2d), following similar approaches applied to sediment cores in the Southern Ocean (e.g., Pahnke et al., 2003; Rose et al., 2010; Waelbroeck et al., 2019). Our age model yields sedimentation rates between 10 and 20 cm/kyr during the last deglaciation. Choosing different SST-δD tie-points will slightly change the calculated deep-water radiocarbon values, but not to a degree that would affect our main conclusion (Figure S2). All uncertainties associated with the age model are computed using the Undatable MATLAB script (Lougheed & Obrochta, 2019), and are incorporated into uncertainty propagation of deep-water radiocarbon signatures.

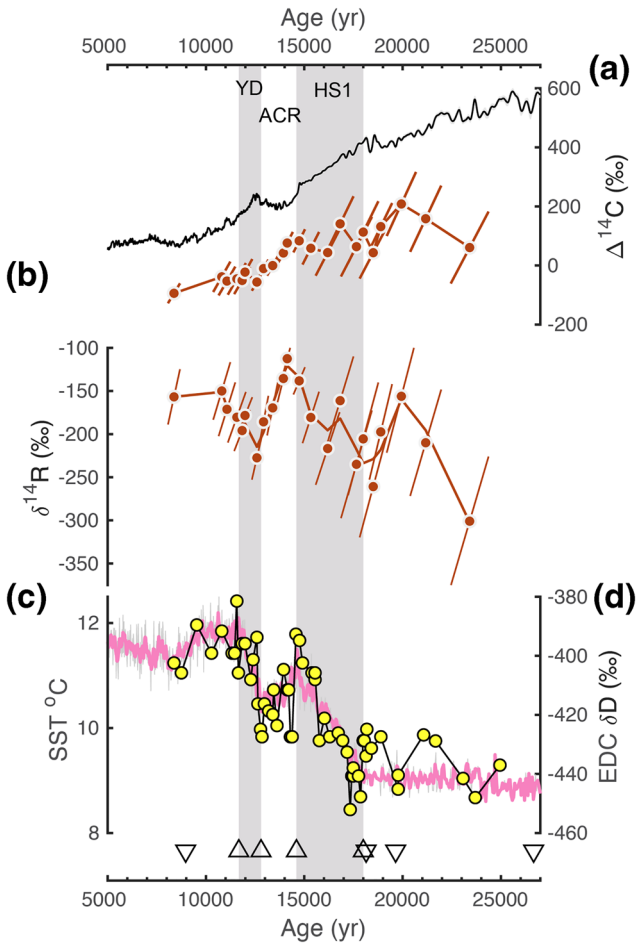

Figure 2. (a) MD97-2106 benthic $\Delta^{14}C$ with ±1σ uncertainties compared to IntCal20 atmospheric $\Delta^{14}C$ (Reimer et al., 2020). (b) MD97-2016 $\delta^{14}R$. (c) MD97-2106 SST reconstruction based on *G. bulloides* Mg/Ca. (d) EDC δD (Jouzel et al., 2007). Upward and downward triangles represent age control points based on SST-δD alignment and planktic radiocarbon dates, respectively. Gray bars indicate the YD and HS1. SST, sea surface temperature. EDC, EPICA Dome C; YD, Younger Dryas; HS, Heinrich Stadial 1.

2.4. Deep-water Radiocarbon Signatures

Foraminiferal radiocarbon measurements were performed at the ANU and the Keck Carbon Cycle AMS Laboratory at the University of California Irvine. Foraminifera shells from the fraction larger than 212 μm were picked. Miliolid species (e.g., *Pyrgo* spp., *Triloculina* spp.) and deep-infaunal species (e.g., *Chilostomella oolina*, *Globobulimina* spp.) were excluded to avoid potential bias on radiocarbon ages (Ezat et al., 2017; Magana et al., 2010). The weight of benthic foraminifera ranges from 2.2 to 4.8 mg per sample, with an average of 3.5 mg. Deep-water $\Delta^{14}C$ is calculated using the following equation (Adkins & Boyle, 1997; Stuiver & Polach, 1977): $\Delta^{14}C_{\text{deep-water}} = \left(\frac{e^{-14\text{C age}/8{,}033}}{e^{-\text{Cal age}/8{,}266}} - 1\right) * 1{,}000$, where ^{14}C age is the measured radiocarbon age for benthic foraminifera and Cal age is the calendar age based on our age model as described above. To account for the influence of atmospheric $\Delta^{14}C$ variabilities on deep water $\Delta^{14}C$, we adopt the metric of $\delta^{14}R$, the relative deviation between deep water and atmospheric $\Delta^{14}C$, which is calculated by the following equation (Hines et al., 2015; Soulet et al., 2016; Zhao & Keigwin, 2018): $\delta^{14}R = \left(\frac{\frac{\Delta^{14}C_{\text{deep-water}}}{1{,}000} + 1}{\frac{\Delta^{14}C_{\text{atm}}}{1{,}000} + 1} - 1\right) * 1{,}000$. The 1σ uncertainties of $\Delta^{14}C$ and $\delta^{14}R$ are derived by a Monte-Carlo method, incorporating uncertainties from ^{14}C age measurements, Cal age, and atmospheric $\Delta^{14}C$ (Reimer et al., 2020).

3. Results

3.1. Deep-water $\Delta^{14}C$ and $\delta^{14}R$ at MD97-2106

Our high-resolution radiocarbon record reveals ventilation changes in the deep Southwest Pacific during the last deglaciation on millennial timescales, with errors including uncertainties associated with radiocarbon measurements in benthic foraminifera, age model, and atmospheric radiocarbon. From the LGM to HS1 (22–14.6 kyr BP), benthic foraminiferal $\Delta^{14}C$ at MD97-2106 remained roughly stable, while atmospheric $\Delta^{14}C$ decreased (Figure 2a). During the ACR, MD97-2106 benthic $\Delta^{14}C$ dropped by ~150‰, while atmospheric $\Delta^{14}C$ was relatively stable. From the YD to the early Holocene, our deep-water $\Delta^{14}C$ stayed constant, coinciding with the declining atmospheric $\Delta^{14}C$ (Figure 2a). Considering atmospheric and benthic $\Delta^{14}C$ changes together, our calculated $\delta^{14}R$ at

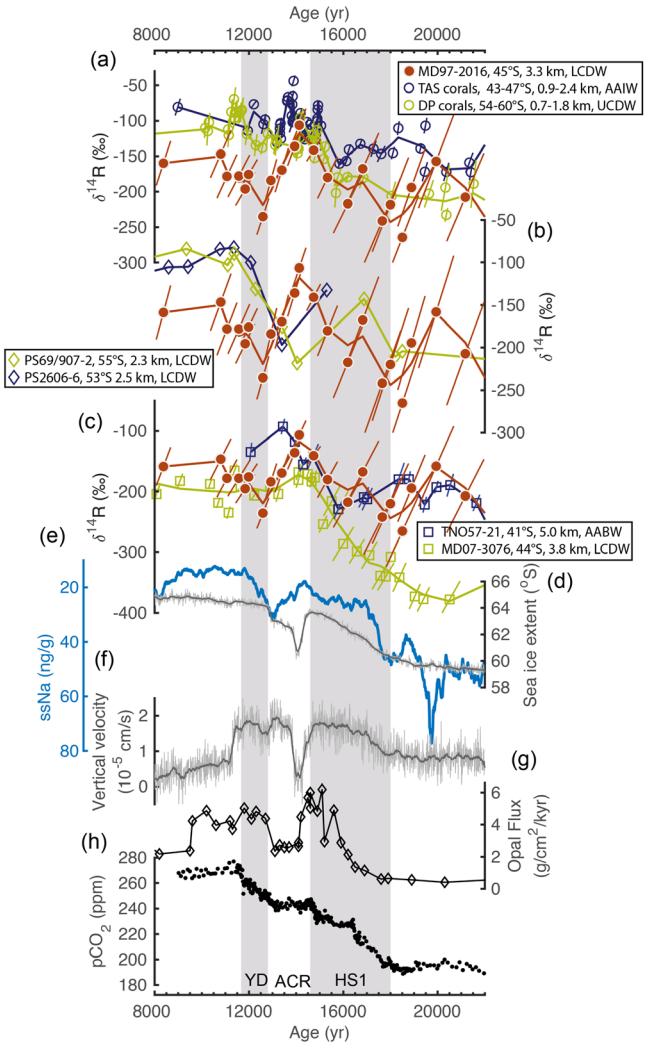

Figure 3. Comparison of MD97-2016 $\delta^{14}R$ with (a) deep-sea coral records (Burke & Robinson, 2011; Chen et al., 2015; Hines et al., 2015) from the South Pacific, (b) benthic foraminifera based records from the South Indian (Ronge et al., 2020), (c) benthic foraminifera based records from the South Atlantic (Barker et al., 2010; Skinner et al., 2010). (d) Zonal average of permanent sea-ice extent (70% ice concentration) in the Pacific Sector of the Southern Ocean from CCSM3-TRaCE-21ka (Liu et al., 2009). (e) Sea-salt sodium at West Antarctic Ice Sheet (15-point moving average) (EPICA Community Members, 2013). (f) Zonal average of vertical velocity at the bottom of mixed layer at 68°S in the Pacific from CCSM3-TRaCE-21ka (Liu et al., 2009). (g) Opal flux in the Antarctic Zone (Anderson et al., 2009). (h) Atmospheric CO_2 (Marcott et al., 2014). Curves in (a–c) are LOESS-smoothed averages. Bold curves in (d) and (f) are 100 years moving averages.

MD97-2106 were more depleted, by ~70‰, during the LGM than during the early Holocene (Figure 2b). Our $\delta^{14}R$ increased by ~100‰ during HS1, peaked at the onset of the ACR, and declined by ~80‰ during the ACR. This was followed by a ~60‰ rise during the YD (Figure 2b). The $\delta^{14}R$ decline across the ACR is a robust feature that is independent of the choice of the tie-points for the ACR in our age model (Figure S2). Even if the tie-points are offset by 2–5 cm, the $\delta^{14}R$ structure during the ACR remains unchanged, despite that the magnitude of $\delta^{14}R$ would vary between 50‰ and 150‰ (Figure S2). Such a clear $\delta^{14}R$ decline during the ACR is a unique feature compared to other records in the deep Southern Ocean based on both deep-sea corals and benthic foraminifera.

3.2. Comparison With Southern Ocean Deep-Sea Coral Records

Figure 3a shows deep-sea coral $\delta^{14}R$ records from South of Tasmania (AAIW depth) and the Drake Passage (UCDW depth) (Burke & Robinson, 2011; Chen et al., 2015; Hines et al., 2015). During the LGM, MD97-2106 benthic foraminifera and Drake Passage deep-sea corals show similar $\delta^{14}R$ values that are ~70‰ more depleted than AAIW signatures revealed by South Tasmania deep-sea corals. During HS1, both LCDW (MD97-2106) and UCDW (Drake Passage) $\delta^{14}R$ increased and converged with the AAIW $\delta^{14}R$ record (South Tasmania). $\delta^{14}R$ at MD97-2106 declined by ~80‰ during the ACR. In contrast, average $\delta^{14}R$ in UCDW and AAIW show minimal changes between the onset and the end of the ACR, despite large centennial-timescale variabilities within the ACR. As a result, a ~100‰ $\delta^{14}R$ gradient between UCDW and LCDW can be inferred by the end of ACR. To our knowledge, the diverging ACR radiocarbon signals between LCDW and UCDW is observed for the first time in the South Pacific.

3.3. Comparison With Other Southern Ocean Benthic Foraminiferal Records

Figures 3b and 3c show $\delta^{14}R$ records in two Indian cores PS39/907-2 and PS2606-6 (53–55°S, 2.3–2.5 km; LCDW-depth) (Ronge et al., 2020) and two Atlantic cores TNO57-21 (41°S, 5.0 km; AABW depth) (Barker et al., 2010) and MD07-3076 (44°S, 3.8 km; LCDW depth) (Skinner et al., 2010). For the two Atlantic cores, we show $\delta^{14}R$ records based on their original age models. Applying updated age models to these two cores (Waelbroeck et al., 2019) does not affect our conclusion (Figure S3). During the LGM, our $\delta^{14}R$ data are similar to those from TNO57-21 and PS69/907-2, but are higher than values from MD07-3076 (Figures 3b and 3c). During HS1, deep-water $\delta^{14}R$ at MD97-2106 converged with all other $\delta^{14}R$ records investigated (Figures 3b and 3c). During the ACR, compared to the MD97-2106 record that shows a well-defined ~80‰ $\delta^{14}R$ decline, the two Indian records show ambiguous trends due to their low resolution (Figure 3b). In the Atlantic, the ACR $\delta^{14}R$ structure in core TNO57-21 is sensitive to the choice of age model: while there is minimal change when using the original age model (Figure 3), a ~30‰ decline can be observed using the age model of Waelbroeck et al. (2019)(Figure S3). At MD07-3076, ~50‰–70‰ declines may be revealed depending on different age models (Figure S3). During the YD, the two Indian cores show increases in $\delta^{14}R$ similar to our MD97-2106 record. $\delta^{14}R$ changes during the YD at the two Atlantic cores are also dependent on the choice of age models. At TNO57-21, an increase in $\delta^{14}R$ can only be observed using the age model of Waelbroeck et al. (2019). At MD07-3076, while no clear trend

in $\delta^{14}R$ is seen using the original age model, a ~60‰ $\delta^{14}R$ increase can be obtained using the age model of Waelbroeck et al. (2019) (Figure S3).

4. Discussion

4.1. Breakdown of Southern Ocean Stratification During HS1

During the LGM, our new record of LCDW $\delta^{14}R$ from the Southwest Pacific (MD97-2106) is similar to many other records of deep water masses from the Southern Ocean (Barker et al., 2010; Burke & Robinson, 2011; Chen et al., 2015; Ronge et al., 2020) (Figures 3a–3c), but shows lower values than reconstructions of nearby Southwest Pacific intermediate waters (Hines et al., 2015) (Figure 3a). Among the deep-water $\delta^{14}R$ records, the South Atlantic site MD07-3076 has the most negative $\delta^{14}R$ values during the LGM, although sensitivity test suggests this LGM $\delta^{14}R$ value is sensitive to the choices of age models (Figure S3). Nevertheless, the most negative $\delta^{14}R$ at MD07-3076 can be attributed to an influence from poorly ventilated Pacific Deep Waters, as indicated by deep water $[CO_3^{2-}]$ and neodymium isotopes (Yu et al., 2020). Our $\delta^{14}R$ record, taken together with published records, suggests that the deep Southern Ocean became more isolated from the upper ocean and the atmosphere during the LGM. This would facilitate sequestration of carbon in the ocean interior with an effect to lower atmospheric CO_2 (Burke & Robinson, 2011; Rae et al., 2018; Skinner et al., 2010).

During HS1, our $\delta^{14}R$ from the Southwest Pacific increased, in parallel with other deep Southern Ocean water mass records (Barker et al., 2010; Burke & Robinson, 2011; Chen et al., 2015; Ronge et al., 2020; Skinner et al., 2010) (Figures 3a–3c), converging with nearby coral $\delta^{14}R$ records at intermediate depths (Hines et al., 2015) (Figure 3a). This convergence of deep and intermediate seawater $\delta^{14}R$ indicates a breakdown of stratification between intermediate and deep water masses. Similar features are also observed in other sectors of the Southern Ocean, suggesting widespread water mass de-stratification during HS1. This early deglacial breakdown in stratification might have enhanced nutrient supply and fueled surface production in the Antarctic Zone, consistent with proxy records (Anderson et al., 2009). At the same time, improved Southern Ocean ventilation would release old carbon to the atmosphere during HS1, contributing to the millennial timescale atmospheric CO_2 rise (Anderson et al., 2009; Sigman et al., 2010; Stephens & Keeling, 2000; Toggweiler et al., 2006).

4.2. Reduced Deep Southern Ocean Ventilation During the ACR

In contrast to the rise in LCDW $\delta^{14}R$ that is consistent with stratification breakdown during HS1, our reconstruction of LCDW $\delta^{14}R$ in the Southwest Pacific differs from many other records during the ACR (Figures 3a–3c). It decreased by ~80‰ during this period, indicating deteriorating ventilation of the deep Southwest Pacific. We note that previous LCDW $\delta^{14}R$ records from the Indian Sector also show low $\delta^{14}R$ values during the ACR, but no clear trend can be defined, owing to the limited resolution (Figure 3b) (Ronge et al., 2020). By contrast, our record, for the first time, clearly defines a declining trend at LCDW-depths in the deep Southern Ocean during the ACR, filling a critical gap.

The clear decline in LCDW $\delta^{14}R$ during the ACR observed at our core differs from $\delta^{14}R$ at UCDW-depths and AAIW-depths in the South Pacific, which shows sustained high $\delta^{14}R$ values despite some short-lived variabilities (Burke & Robinson, 2011; Chen et al., 2015; Hines et al., 2015) (Figure 3a). The increased gradient in UCDW-LCDW $\delta^{14}R$ during the ACR indicates a re-establishment of strong stratification in the deep Southern Ocean between UCDW and LCDW during this period. Furthermore, on millennial timescales, the increased UCDW-LCDW stratification is synchronous with the widespread mid-high latitude Southern Hemisphere cooling (Pedro et al., 2015), and sea-ice expansion around Antarctica (Lamping et al., 2020; EPICA Community Members, 2013). Such a coincidence suggests that the deterioration of the deep Southwest Pacific ventilation and the establishment of the deep Southern Ocean stratification are likely linked to the Southern Hemisphere changes.

The lowering of LCDW $\delta^{14}R$ and the apparent increase in UCDW-LCDW stratification during the ACR we observe can be explained by changes in Antarctic sea-ice. Expanded sea-ice reduces communication between deep and surface waters (Nadeau et al., 2019; Sigman et al., 2010; Stephens & Keeling, 2000) and

increases the density contrast between the upper and lower ocean circulation cells (Ferrari et al., 2014; Nadeau et al., 2019; Watson & Garabato, 2006; Watson et al., 2015). Modeling results (CCSM3-TraCE-21ka) also demonstrate a link between perennial sea-ice expansion during the ACR and reduced deep vertical Southern Ocean mixing (Liu et al., 2009) (Figures 3d and 3f). Furthermore, the extent of Southern Ocean sea-ice also dictates the depth of the boundary separating these two circulation cells in the ocean interior (Ferrari et al., 2014; Nadeau et al., 2019; Watson & Garabato, 2006; Watson et al., 2015), so that sea-ice expansion is proportional to the depth that the boundary between the upper and lower circulation cells shoals (Ferrari et al., 2014; Nadeau et al., 2019). Indeed, ice core sea-salt sodium records show increased sea-ice production during the ACR relative to HS1 (EPICA Community Members, 2013) (Figure 3e), and In regions like the western Amundsen Sea, the sea-ice coverage during the ACR is even thought to reach a similar latitude to that during the LGM on a local scale (Lamping et al., 2020). The sea-ice expansion during the ACR reduced gas exchange between the atmosphere and the deep Southern Ocean, thus resulting in radiocarbon aging of LCDW during the ACR (Nadeau et al., 2019). Additionally, the sea-ice was overall less extensive during the ACR than the LGM (EPICA Community Members, 2013), the boundary between two circulation cells would be deeper during the ACR than the LGM as a result. These predictions of expanded Southern Ocean sea-ice during the ACR are consistent with our results that demonstrate a large $\delta^{14}R$ contrast between UCDW and LCDW and thus a deeper stratification in the Southern Ocean during the ACR (Figure 3a).

4.2.1. Interbasin Differences in the ACR Ventilation

Ventilation changes in the deep Southern Ocean during the ACR appear to differ among three sectors, based on currently available data. Records from the Southwest Pacific (this study) and Indian Sectors (Ronge et al., 2020) demonstrate a similar pattern of reduced ventilation and increased stratification during the ACR, although Indian-Sector records with higher resolution are needed to better confirm this agreement. In the Atlantic Sector of the Southern Ocean, a clear trend in ventilation changes during the ACR is still difficult to confirm because of relatively low temporal resolution in Core TNO57-21 (Barker et al., 2010) (Figure 3c) and an age model-sensitive $\delta^{14}R$ at the better resolved Core MD07-3076 (Figures 3c and S3) (Skinner et al., 2010; Waelbroeck et al., 2019). The lack of a clear decrease in $\delta^{14}R$ during the ACR in the South Atlantic (Figure 3c) could be explained by a stronger influence of the relatively well-ventilated (high-$\delta^{14}R$) NADW. Several studies report a reinvigorated NADW during the ACR, which would increase deep water $\delta^{14}R$ throughout the South Atlantic (including sites TNO57-21 and MD07-3076) (Barker et al., 2010; McManus et al., 2004; Skinner et al., 2010, 2013, 2014). An increased NADW influence on the deep South Atlantic during the ACR is also registered by deep-water $[CO_3^{2-}]$ (Yu et al., 2014) and $\delta^{13}C$ records (Lund et al., 2015; Ninnemann & Charles, 2002). Consequently, this enhanced NADW influence may partially counteract the effect from the reduced Southern Ocean ventilation.

The interbasin difference in ventilation changes during the ACR can be attributed to the restricted interbasin connectivity at deep depths which was not relaxed until the onset of the YD (McCave et al., 2008; Sikes et al., 2017). In contrast to the South Atlantic, the influence from the reinvigorated NADW during the ACR on our site from the Southwest Pacific is more limited, so that a larger $\delta^{14}R$ decline can be recorded at site MD97-2106. However, we also note that the limited deep interbasin transport before the YD (McCave et al., 2008; Sikes et al., 2017) may confine regional influence on radiocarbon in the Pacific Sector. Therefore, we cannot entirely rule out the possibility that the large $\delta^{14}R$ decline observed at Core MD97-2106 is partially due to stronger influence from a radiocarbon depleted water mass, e.g., Pacific Deep Water. More high-resolution records with reliable age models are needed to better constrain the deglacial ventilation history in the Southern Ocean.

4.2.2. Influence of Deep Southern Ocean Stratification on Atmospheric CO_2

The reduced ventilation and increased stratification during the ACR in the deep Pacific Sector of the Southern Ocean, inferred from our radiocarbon records, has important implications on the paused atmospheric CO_2 rise during this period. The reduced ventilation and increased stratification tend to store carbon in the deep Southern Ocean. Moreover, these changes also coincide with reduced CO_2 release from the deep Southern Ocean inferred from reduced upwelling in the Antarctic Zone, as indicated by the declining export

productivity (Anderson et al., 2009). Based on these records, more carbon was likely accumulated in the deep Southern Ocean during the ACR, when the atmospheric CO_2 rise was halted (Marcott et al., 2014). Meanwhile, CO_2 outgassing was sustained during this period in regions such as the Eastern Equatorial Pacific, and the North Pacific, based on surface water pH reconstructions (Gray et al., 2018; Martinez-Boti et al., 2015). The increased carbon storage in the deep Southern Ocean, supported by our LCDW $\delta^{14}R$ record, likely counteracted the CO_2 outgassing from other regions, and contributed to the atmospheric CO_2 plateau during the ACR observed in the ice core record (Marcott et al., 2014).

4.3. Enhanced Deep Southwest Pacific Ventilation During the YD

The deep-water $\delta^{14}R$ increase at MD97-2106 during the YD also coincides with a millennial-timescale atmospheric CO_2 increase (Figures 3a and 3h). Our reconstruction fills the observational gap of LCDW radiocarbon during the YD in the South Pacific, and shows that old carbon was released from the deep Southwest Pacific during this time. In contrast, deep-sea coral records show no major $\delta^{14}R$ increase in UCDW until the end of the YD, reflecting minimal ventilation changes to the UCDW characteristics in the Southern Ocean during the YD (Chen et al., 2015). Therefore, our record suggests that the ventilated deep waters in the Pacific Sector of the Southern Ocean are important sources of the millennial-timescale atmospheric CO_2 rise during the YD. The enhanced ventilation is likely the result of breakdown of the ACR stratification, accompanied by the intensified upwelling around Antarctica (Anderson et al., 2009), and sea-ice retreat associated with the South Hemisphere warming (Figures 3d–3f). Similar $\delta^{14}R$ changes during the YD have also been observed in the Indian Sector (Ronge et al., 2020) (Figure 3b). Compared to the Indo-Pacific deep-water radiocarbon records, the South Atlantic data during the YD shows a less clear signal for improved ventilation (Skinner et al., 2010). This may be linked to the lack of strong $\delta^{14}R$ decline during the ACR in the South Atlantic. The South Atlantic likely remained better ventilated than the Indo-Pacific due to the NADW influence during the ACR. As a result, the improvement of the South Atlantic ventilation may be smaller, and/or the deep water radiocarbon is less sensitive to further ventilation enhancement during the YD.

5. Conclusions

We present a new radiocarbon record at the LCDW-depth from the southwest Pacific, with the deglacial age model constrained by tuning planktic Mg/Ca-SST to Antarctic ice-core air temperature. Our data show two-phase ventilation increases that coincided with millennial-timescale atmospheric CO_2 rises during HS1 and the YD. This lends strong support to the important role of the Pacific Sector of the Southern Ocean in affecting millennial-timescale deglacial atmospheric CO_2 rise during these times. Combined with published data, our data also suggest that the deep South Pacific became less well-ventilated and more stratified during the ACR. This is possibly caused by a readvancement of sea-ice in the Southern Ocean, allowing accumulation of carbon at depth. The increased carbon reservoir in the deep Southwest Pacific during the ACR may counteract sustained CO_2 outgassing in other regions, and contributed to the halted atmospheric CO_2 rise during the ACR. Overall, our record demonstrates a close relationship between deep Southern Ocean ventilation and deglacial atmospheric CO_2 variations.

Acknowledgments
We thank Bradley Opdyke and William Howard for providing sediment samples. We thank three reviewers for their constructive comments, which immensely improved this manuscript. Jimin Yu designed this study. Yuhao Dai made trace element measurements, picked foraminifera shells for radiocarbon analyses, and analyzed model output data. Patrick A. Rafter performed radiocarbon analyses. Yuhao Dai wrote the paper with contributions from Jimin Yu and Patrick A. Rafter. This research is supported by NSFC (41676026), ARC Future Fellowship (FT140100993), and ARC Discovery Project (DP190100894) to Jimin Yu, and US National Science Foundation (1635610, 1838751, and 2015647) to Patrick A. Rafter.

Data Availability Statement

New data generated in this study are all in the supplementary material, and are available at https://doi.org/10.5281/zenodo.4419794.

References

Adkins, J. F., & Boyle, E. A. (1997). Changing atmospheric Δ14C and the record of deep water paleoventilation ages. *Paleoceanography and Paleoclimatology*, *12*(3), 337–344. https://doi.org/10.1029/97PA00379

Allen, K. A., Sikes, E. L., Hönisch, B., Elmore, A. C., Guilderson, T. P., Rosenthal, Y., & Anderson, R. F. (2015). Southwest Pacific deep water carbonate chemistry linked to high southern latitude climate and atmospheric CO_2 during the Last Glacial Termination. *Quaternary Science Reviews*, *122*, 180–191. https://doi.org/10.1016/j.quascirev.2015.05.007

Anderson, R. F., Ali, S., Bradtmiller, L. I., Nielsen, S. H. H., Fleisher, M. Q., Anderson, B. E., & Burckle, L. H. (2009). Wind-driven upwelling in the Southern Ocean and the deglacial rise in atmospheirc CO_2. *Science*, *323*(5920), 1443–1448.

Barker, S., Greaves, M., & Elderfield, H. (2003). A study of cleaning procedures used for foraminiferal Mg/Ca paleothermometry. *Geochemistry, Geophysics, Geosystems*, *4*(9), 8407. https://doi.org/10.1029/2003GC000559

Barker, S., Knorr, G., Vautravers, M. J., Diz, P., & Skinner, L. C. (2010). Extreme deepening of the Atlantic overturning circulation during deglaciation. *Nature Geoscience*, *3*(8), 567–571.

Bostock, H. C., Hayward, B. W., Neil, H. L., Sabaa, A. T., & Scott, G. H. (2015). Changes in the position of the Subtropical Front south of New Zealand since the last glacial period. *Paleoceanography and Paleoclimatology*, *30*, 824–844. https://doi.org/10.1002/2014PA002652

Boyle, E., & Keigwin, L. (1985). Comparison of Atlantic and Pacific paleochemical records for the last 215,000 years: Changes in deep ocean circulation and chemical inventories. *Earth and Planetary Science Letters*, *76*(1), 135–150.

Broecker, W. S., Andree, M., Bonani, G., Wolfli, W., Oeschger, H., Klas, M., et al. (1988). Preliminary estimates for the radiocarbon age of deep water in the glacial ocean. *Paleoceanography and Paleoclimatology*, *3*(6), 659–669. https://doi.org/10.1029/PA003i006p00659

Buizert, C., Sigl, M., Severi, M., Markle, B. R., Wettstein, J. J., McConnell, J. R., et al. (2018). Abrupt ice-age shifts in southern westerly winds and Antarctic climate forced from the north. *Nature*, *563*(7733), 681–685. https://doi.org/10.1038/s41586-018-0727-5

Burke, A., & Robinson, L. F. (2011). The Southern Ocean's role in carbon exchange during the last deglaciation. *Science*, *335*(6068), 557–561. https://doi.org/10.1126/science.1208163

Chen, T., Robinson, L. F., Burke, A., Southon, J., Spooner, P., Morris, P. J., & Ng, H. C. (2015). Synchronous centennial abrupt events in the ocean and atmosphere during the last deglaciation. *Science*, *349*(6255), 1537–1541. https://doi.org/10.1126/science.aac6159

Elderfield, H., & Ganssen, G. (2000). Past temperature and δ18O of surface ocean waters inferred from foraminiferal Mg/Ca ratios. *Nature*, *405*(6785), 442–445.

Ezat, M. M., Rasmussen, T. L., Thornalley, D. J. R., Olsen, J., Skinner, L. C., Hönisch, B., & Groeneveld, J. (2017). Ventilation history of Nordic Seas overflows during the last (de)glacial period revealed by species-specific benthic foraminiferal14C dates. *Paleoceanography and Paleoclimatology*, *32*, 172–181. https://doi.org/10.1002/2016PA003053

Farneti, R., Downes, S. M., Griffies, S. M., Marsland, S. J., Behrens, E., Bentsenf, M., et al. (2015). An assessment of Antarctic Circumpolar Current and Southern Ocean meridional overturning circulation during 1958–2007 in a suite of interannual CORE-II simulations. *Ocean Modelling*, *93*, 84–120. https://doi.org/10.1016/j.ocemod.2015.07.009

Ferrari, R., Jansen, M. F., Adkins, J. F., Burke, A., Stewart, A. L., & Thompson, A. F. (2014). Antarctic sea ice control on ocean circulation in present and glacial climates. *Proceedings of the National Academy Sciences of the United States of America*, *111*(24), 8753–8758. https://doi.org/10.1073/pnas.1323922111

Ganachaud, A. (2003). Large-scale mass transports, water mass formation, and diffusivities estimated from World Ocean Circulation Experiment (WOCE) hydrographic data. *Journal of Geophysical Research*, *108*(C7). 3213. https://doi.org/10.1029/2002JC001565

Gray, W. R., Rae, J. W. B., Wills, R. C. J., Shevenell, A. E., Taylor, B., Burke, A., et al. (2018). Deglacial upwelling, productivity and CO_2 outgassing in the North Pacific Ocean. *Nature Geoscience, 11*, 340–344. https://doi.org/10.1038/s41561-018-0108-6

Greaves, M., Caillon, N., Rebaubier, H., Bartoli, G., Cacho, I., Clarke, L., et al. (2008). Interlaboratory comparison study of calibration standards for foraminiferal Mg/Ca thermometry. *Geochemistry, Geophysics, Geosystems*, *9*, Q08010. https://doi.org/10.1029/2008GC001974

Hines, S. K. V., Southon, J. R., & Adkins, J. F. (2015). A high-resolution record of Southern Ocean intermediate water radiocarbon over the past 30,000 years. *Earth and Planetary Science Letters*, *432*, 46–58. https://doi.org/10.1016/j.epsl.2015.09.038

Jouzel, J., Masson-Delmotte, V., Cattani, O., Dreyfus, G., Falourd, S., Hoffmann, G., et al.(2007). Orbital and millennial Antarctic climate variability over the past 800,000 years. *Science*, *317*(5839), 793–796.

Key, R. M., Kozyr, A., Sabine, C. L., Lee, K., Wanninkhof, R., Bullister, J. L., et al. (2004). A global ocean carbon climatology: Results from Global Data Analysis Project (GLODAP). *Global Biogeochemical Cycles*, *18,* GB4031. https://doi.org/10.1029/2004GB002247

Lamping, N., Müller, J., Esper, O., Hillenbrand, C.-D., Smith, J. A., & Kuhn, G. (2020). Highly branched isoprenoids reveal onset of deglaciation followed by dynamic sea-ice conditions in the western Amundsen Sea, Antarctica. *Quaternary Science Reviews*, *228*, 106103. https://doi.org/10.1016/j.quascirev.2019.106103

Lee, S. K., Lumpkin, R., Baringer, M. O., Meinen, C. S., Goes, M., Dong, S., et al. (2019). Global meridional overturning circulation inferred from a data-constrained ocean & sea-ice model. *Geophysical Research Letters*, *46*, 1521–1530. https://doi.org/10.1029/2018GL080940

Liu, Z., Otto-Bliesner, B. L., He, F., Brady, E. C., Tomas, R., Clark, P. U., et al. (2009). Transient simulation of last deglaciation with a new mechanism for Bolling-Allerod warming. *Science*, *325*(5938), 310–314. https://doi.org/10.1126/science.1171041

Lizarralde, D., Soule, S. A., Seewald, J. S., & Proskurowski, G. (2010). Carbon release by off-axis magmatism in a young sedimented spreading center. *Nature Geoscience*, *4*(1), 50–54. https://doi.org/10.1038/ngeo1006

Lougheed, B. C., & Obrochta, S. P. (2019). A rapid, deterministic age-depth modeling routine for geological sequences with inherent depth uncertainty. *Paleoceanography and Paleoclimatology*, *34*(1), 122–133. https://doi.org/10.1029/2018pa003457

Lund, D. C., Tessin, A. C., Hoffmann, J., & Schmittner, A. (2015). Southwest Atlantic water mass evolution during the last deglaciation. *Paleoceanography and Paleoclimatology*, *30*, 477–494. https://doi.org/10.1002/2014PA002657

Magana, A. L., Southon, J. R., Kennett, J. P., Roark, E. B., Sarnthein, M., & Stott, L. D. (2010). Resolving the cause of large differences between deglacial benthic foraminifera radiocarbon measurements in Santa Barbara Basin. *Paleoceanography and Paleoclimatology*, *25*, PA4102. https://doi.org/10.1029/2010PA002011

Marcott, S. A., Bauska, T. K., Buizert, C., Steig, E. J., Rosen, J. L., Cuffey, K. M, et al. (2014). Centennial-scale changes in the global carbon cycle during the last deglaciation. *Nature*, *514*(7524), 616–619. https://doi.org/10.1038/nature13799

Martinez-Boti, M. A., Marino, G., Foster, G. L., Ziveri, P., Henehan, M. J., Rae, J. W., et al. (2015). Boron isotope evidence for oceanic carbon dioxide leakage during the last deglaciation. *Nature*, *518*(7538), 219–222. https://doi.org/10.1038/nature14155

McCave, I. N., Carter, L., & Hall, I. R. (2008). Glacial–interglacial changes in water mass structure and flow in the SW Pacific Ocean. *Quaternary Science Reviews*, *27*(19–20), 1886–1908. https://doi.org/10.1016/j.quascirev.2008.07.010

McManus, J., Francois, R., Gherardi, J. M., Keigwin, L., & Brown-Leger, S. (2004). Collapse and rapid resumption of Atlantic meridional circulation linked to deglacial climate changes. *Nature*, *428*(6985), 834–837.

Members, E. C. (2006). One-to-one coupling of glacial climate variability in Greenland and Antarctica. *Nature*, *444*(7116), 195–198. https://doi.org/10.1038/nature05301

Members, W. D. P. (2013). Onset of deglacial warming in West Antarctica driven by local orbital forcing. *Nature*, *500*(7463), 440–444. https://doi.org/10.1038/nature12376

Monnin, E., Indermuhle, A., Dallenbach, A., Fluckiger, J., Stauffer, B., Stocker, T. F., et al. (2001). Atmospheric CO_2 concentrations over the last glacial termination. *Science*, *291*(5501), 112–114. https://doi.org/10.1126/science.291.5501.112

Moy, A., Howard, W., & Gagan, K. (2006). Late quaternary paleoceanography of the circumpolar deep water from the South Tasman Rise. *Journal of Quaternary Science*, *21*(7), 763–777. https://doi.org/10.1002/jqs.1067

Nadeau, L.-P., Ferrari, R., & Jansen, M. F. (2019). Antarctic sea ice control on the depth of North Atlantic deep water. *Journal of Climate*, *32*(9), 2537–2551. https://doi.org/10.1175/jcli-d-18-0519.1

Ninnemann, U., & Charles, C. D. (2002). Changes in the mode of Southern Ocean circulation over the last glacial cycle revealed by foraminiferal stable isotopic variability. *Earth and Planetary Science Letters*, *201*, 383–396.

Pahnke, K., Zahn, R., Elderfield, H., & Schulz, M. (2003). 340,000-Year Centennial-Scale Marine Record of Southern Hemisphere Climatic Oscillation. *Science*, *301*, 948–952.

Pedro, J. B., Bostock, H. C., Bitz, C. M., He, F., Vandergoes, M. J., Steig, E. J., et al. (2015). The spatial extent and dynamics of the Antarctic Cold Reversal. *Nature Geoscience, 9*, 51–55. https://doi.org/10.1038/ngeo2580

Petit, J.-R., Jouzel, J., Raynaud, D., Barkov, N. I., Barnola, J.-M., Basile, I., et al. (1999). Climate and atmospheric history of the past 420,000 years from the Vostok ice core, Antarctica. *Nature*, *399*(6735), 429–436.

Rae, J. W. B., Burke, A., Robinson, L. F., Adkins, J. F., Chen, T., Cole, C., et al. (2018). CO_2 storage and release in the deep Southern Ocean on millennial to centennial timescales. *Nature*, *562*(7728), 569–573. https://doi.org/10.1038/s41586-018-0614-0

Rafter, P. A., Carriquiry, J. D., Herguera, J. C., Hain, M. P., Solomon, E. A., & Southon, J. R. (2019). Anomalous >2000 year old surface ocean radiocarbon age as evidence for deglacial geologic carbon release. *Geophysical Research Letters, 46*, 13950–13960. https://doi.org/10.1029/2019GL085102

Rafter, P. A., Herguera, J.-C., & Southon, J. R. (2018). Extreme lowering of deglacial seawater radiocarbon recorded by both epifaunal and infaunal benthic foraminifera in a wood-dated sediment core. *Climate of the Past*, *14*(12), 1977–1989. https://doi.org/10.5194/cp-14-1977-2018

Reimer, P. J., Austin, W. E. N., Bard, E., Bayliss, A., Blackwell, P. G., Ramsey, C. B., et al. (2020). The IntCal20 northern hemisphere radiocarbon age calibration curve (0–55 cal kBP). *Radiocarbon*, *62*(4), 725–757. https://doi.org/10.1017/rdc.2020.41

Rintoul, S. R. (2018). The global influence of localized dynamics in the Southern Ocean. *Nature*, *558*(7709), 209–218. https://doi.org/10.1038/s41586-018-0182-3

Ronge, T. A., Prange, M., Mollenhauer, G., Ellinghausen, M., Kuhn, G., & Tiedemann, R. (2020). Radiocarbon evidence for the contribution of the southern indian ocean to the evolution of atmospheric CO_2 over the last 32,000 years. *Paleoceanography and Paleoclimatology*, *35*, e2019PA003733. https://doi.org/10.1029/2019PA003733

Ronge, T. A., Tiedemann, R., Lamy, F., Kohler, P., Alloway, B. V., De Pol-Holz, R., et al. (2016). Radiocarbon constraints on the extent and evolution of the South Pacific glacial carbon pool. *Nature Communications*, *7*, 11487. https://doi.org/10.1038/ncomms11487

Rose, K. A., Sikes, E. L., Guilderson, T. P., Shane, P., Hill, T. M., Zahn, R., & Spero, H. J. (2010). Upper-ocean-to-atmosphere radiocarbon offsets imply fast deglacial carbon dioxide release. *Nature*, *466*(7310), 1093–1097. https://doi.org/10.1038/nature09288

Sarmiento, J., & Toggweiler, J. (1984). A new model for the role of the oceans in determining atmospheric pCO_2. *Nature*, *308*(5960), 621–624.

Siani, G., Michel, E., De Pol-Holz, R., Devries, T., Lamy, F., Carel, M., et al. (2013). Carbon isotope records reveal precise timing of enhanced Southern Ocean upwelling during the last deglaciation. *Nature Communications*, *4*, 2758. https://doi.org/10.1038/ncomms3758

Sigman, D. M., & Boyle, E. A. (2000). Glacial/interglacial variations in atmospheric carbon dioxide. *Nature*, *407*, 859–869.

Sigman, D. M., Hain, M. P., & Haug, G. H. (2010). The polar ocean and glacial cycles in atmospheric CO_2 concentration. *Nature*, *466*(7302), 47–55. https://doi.org/10.1038/nature09149

Sikes, E. L., Allen, K. A., & Lund, D. C. (2017). Enhanced δ13C and δ18O differences between the south Atlantic and south pacific during the last glaciation: The deep gateway hypothesis. *Paleoceanography and Paleoclimatology*, *32*, 1000–1017. https://doi.org/10.1002/2017PA003118

Sikes, E. L., Cook, M. S., & Guilderson, T. P. (2016). Reduced deep ocean ventilation in the Southern Pacific Ocean during the last glaciation persisted into the deglaciation. *Earth and Planetary Science Letters*, *438*, 130–138. https://doi.org/10.1016/j.epsl.2015.12.039

Sikes, E. L., & Guilderson, T. P. (2016). Southwest Pacific Ocean surface reservoir ages since the last glaciation: Circulation insights from multiple-core studies. *Paleoceanography and Paleoclimatology, 31*, 298–310. https://doi.org/10.1002/2015PA002855

Sikes, E. L., Howard, W. R., Samson, C. R., Mahan, T. S., Robertson, L. G., & Volkman, J. K. (2009). Southern Ocean seasonal temperature and Subtropical Front movement on the South Tasman Rise in the late Quaternary. *Paleoceanography and Paleoclimatology*, *24*, PA2201. https://doi.org/10.1029/2008PA001659

Sikes, E. L., Samson, C. R., Guilderson, T. P., & Howard, W. R. (2000). Old radiocarbon ages in the southwest Pacific Ocean during the last glacial period and deglaciation. *Nature*, *405*(6786), 555–559.

Skinner, L. C., Fallon, S., Waelbroeck, C., Michel, E., & Barker, S. (2010). Ventilation of the deep Southern Ocean and deglacial CO_2 rise. *Science*, *328*(5982), 1147–1151. https://doi.org/10.1126/science.1183627

Skinner, L., McCave, I. N., Carter, L., Fallon, S., Scrivner, A. E., & Primeau, F. (2015). Reduced ventilation and enhanced magnitude of the deep Pacific carbon pool during the last glacial period. *Earth and Planetary Science Letters*, *411*, 45–52. https://doi.org/10.1016/j.epsl.2014.11.024

Skinner, L. C., Primeau, F., Freeman, E., de la Fuente, M., Goodwin, P. A., Gottschalk, J., et al. (2017). Radiocarbon constraints on the glacial ocean circulation and its impact on atmospheric CO_2. *Nature Communications*, *8*, 16010. https://doi.org/10.1038/ncomms16010

Skinner, L. C., Scrivner, A. E., Vance, D., Barker, S., Fallon, S., & Waelbroeck, C. (2013). North Atlantic versus Southern Ocean contributions to a deglacial surge in deep ocean ventilation. *Geology*, *41*(6), 667–670. https://doi.org/10.1130/g34133.1

Skinner, L. C., Waelbroeck, C., Scrivner, A. E., & Fallon, S. J. (2014). Radiocarbon evidence for alternating northern and southern sources of ventilation of the deep Atlantic carbon pool during the last deglaciation. *Proceedings of the National Academy Sciences of the United States of America*, *111*(15), 5480–5484. https://doi.org/10.1073/pnas.1400668111

Sokolov, S., & Rintoul, S. R. (2002). Structure of Southern Ocean fronts at 140 degrees E. *Journal of Marine Systems*, *37*(1–3), 151–184. https://doi.org/10.1016/S0924-7963(02)00200-2

Soulet, G., Skinner, L. C., Beaupré, S. R., & Galy, V. (2016). A note on reporting of reservoir 14 C disequilibria and age offsets. *Radiocarbon*, *58*(1), 205–211.

Stephens, B. B., & Keeling, R. F. (2000). The influence of Antarctic sea ice on glacial-interglacial CO_2 variations. *Nature*, *404*(6774), 171–174.

Stott, L., Davy, B., Shao, J., Coffin, R., Pecher, I., Neil, H., et al. (2019). CO_2 release from pockmarks on the Chatham rise-bounty trough at the glacial termination. *Paleoceanography and Paleoclimatology*, *34*, 1726–1743. https://doi.org/10.1029/2019PA003674

Stuiver, M., & Polach, H. A. (1977). Discussion reporting of 14C Data. *Radiocarbon*, *19*(3), 355–363. https://doi.org/10.1017/s0033822200003672

Talley, L. D. (2011). *Descriptive physical oceanography: An introduction*. Amsterdam: Academic Press.

Talley, L. (2013). Closure of the global overturning circulation through the Indian, Pacific, and Southern Oceans: Schematics and transports. *Oceanography*, *26*(1), 80–97. https://doi.org/10.5670/oceanog.2013.07

Toggweiler, J. R., Russell, J. L., & Carson, S. R. (2006). Midlatitude westerlies, atmospheric CO_2, and climate change during the ice ages. *Paleoceanography and Paleoclimatology*, *21*, PA2005. https://doi.org/10.1029/2005PA001154

Waelbroeck, C., Lougheed, B. C., Vazquez Riveiros, N., Missiaen, L., Pedro, J., Dokken, T., et al. (2019). Consistently dated Atlantic sediment cores over the last 40 thousand years. *Scientific Data*, *6*(1), 165. https://doi.org/10.1038/s41597-019-0173-8

Watson, A. J., & Garabato, A. C. N. (2006). The role of Southern Ocean mixing and upwelling in glacial-interglacial atmospheric CO2 change. *Tellus Series B Chemical and Physical Meteorology*, *58*(1), 73–87. https://doi.org/10.1111/j.1600-0889.2005.00167.x

Watson, A. J., Vallis, G. K., & Nikurashin, M. (2015). Southern Ocean buoyancy forcing of ocean ventilation and glacial atmospheric CO_2. *Nature Geoscience, 8*, 861–864. https://doi.org/10.1038/ngeo2538

Yu, J., Anderson, R. F., Jin, Z., Menviel, L., Zhang, F., Ryerson, F. J., & Rohling, E. J. (2014). Deep South Atlantic carbonate chemistry and increased interocean deep water exchange during last deglaciation. *Quaternary Science Reviews*, *90*, 80–89. https://doi.org/10.1016/j.quascirev.2014.02.018

Yu, J., Broecker, W. S., Elderfield, H., Jin, Z., McManus, J. F., & Zhang, F. (2010). Loss of carbon from the deep sea since the LGM. *Science*, *330*, 1084–1087.

Yu, J., Day, J., Greaves, M., & Elderfield, H. (2005). Determination of multiple element/calcium ratios in foraminiferal calcite by quadrupole ICP-MS. *Geochemistry, Geophysics, Geosystems*, *6*, Q08P01. https://doi.org/10.1029/2005GC000964

Yu, J., Elderfield, H., Greaves, M., & Day, J. (2007). Preferential dissolution of benthic foraminiferal calcite during laboratory reductive cleaning. *Geochemistry, Geophysics, Geosystems*, *8*, Q06016. https://doi.org/10.1029/2006GC001571

Yu, J., Menviel, L., Jin, Z. D., Anderson, R. F., Jian, Z., Piotrowski, A. M., et al. (2020). Last glacial atmospheric CO_2 decline due to widespread Pacific deep-water expansion. *Nature Geoscience*, *13*, 628–633. https://doi.org/10.1038/s41561-020-0610-5

Zhao, N., & Keigwin, L. D. (2018). An atmospheric chronology for the glacial-deglacial Eastern Equatorial Pacific. *Nature Communications*, *9*(1), 3077. https://doi.org/10.1038/s41467-018-05574-x